Supporting Information

Novel hydroxylated boron nitride functionalized p-phenylenediamine-grafted graphene: An excellent filler for enhancing the barrier properties of polyurethane

Xuyang Li,[a,b] Parthasarathi Bandyopadhyay,[a] Tolendra Kshetri,[a] Nam Hoon Kim,[a] Joong Hee Lee [a,c*]

[a] Advanced Materials Institute of BIN Convergence Technology (BK21 Plus Global) & Dept. of BIN Convergence Technology, Chonbuk National University, Jeonju, Jeonbuk, 54896, Republic of Korea

[b] School of Chemistry and Pharmaceutical Engineering, Nanyang Normal University, Nanyang, 473061, China

[c] Carbon Composite Research Centre, Department of Polymer - Nano Science and Technology, Chonbuk National University, Jeonju, Jeonbuk, 54896, Republic of Korea

*Corresponding author: E-mail address: jhl@chonbuk.ac.kr (Joong Hee Lee)

**Corresponding author:* Fax: +82 63 270 2341; Tel: +82 63 270 2342

Email address: jhl@chonbuk.ac.kr (Prof. J. H. Lee)

Preparation of graphene oxide (GO)

Modified Hummers method was used to prepare graphite oxide [S1-S3]. At first, 46 ml of concentrated sulfuric was poured in a round-bottom flask and was allowed to stir with a stirring bar. The temperature of the reaction mixture was kept 0-5 ^{o}C during the reaction period using an ice bath. Then, 1 g of sodium nitrate and 2 g of graphite (<20 μm) powder were added in sulfuric acid solution. Next, about 6 g potassium permanganate was added very slowly during the time span of 30 minutes into the round-bottom flask with continuous stirring and the reaction mixture was allowed to stir for another 2 h. After that, the ice bath was removed and the round-bottom flask was transferred to an oil bath at 35 ^{o}C and allowed to stir for another 6 h to make a thick paste. Then, 92 mL of deionized (DI) water was gently poured into the reaction mixture and stirred for 1 h. The bright-yellow reaction mixture was diluted with 280 mL of DI water and followed by addition of 3 mL (30%) hydrogen peroxide. A dilute solution of hydrochloric acid was added to the reaction mixture to remove excess manganese salt. After that, the reaction mixture was repeatedly centrifuged and re-dispersed in DI water several times until the pH of the supernatant solution was natural. Finally, the supernatant solution, which had an ultrasonic treatment for 1 h, was dried by the frozen dryer, and obtained GO.

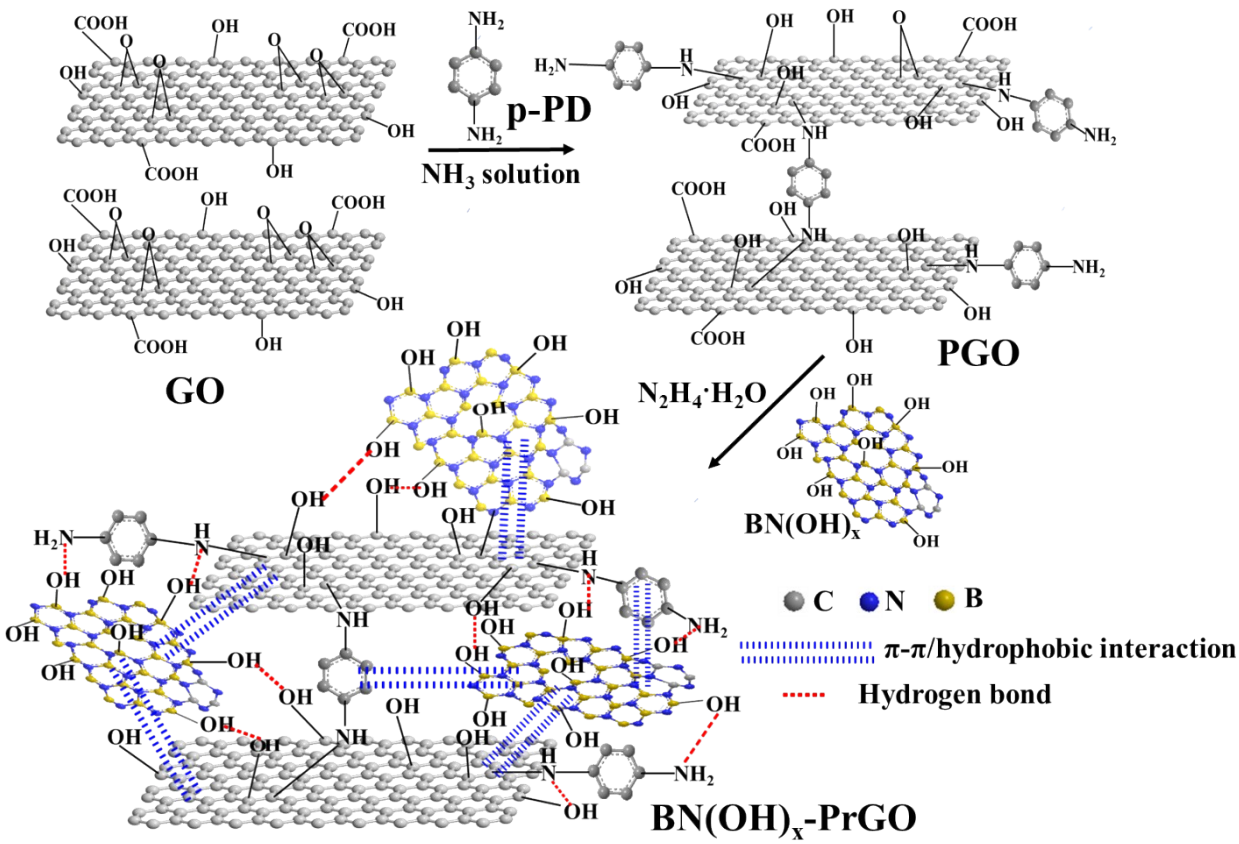

Fig. S1. Schematic illustration of the preparation of $BN(OH)_x$-PrGO filler. ('H' attached to the surface functional group is only shown to make the image more simple and clear).

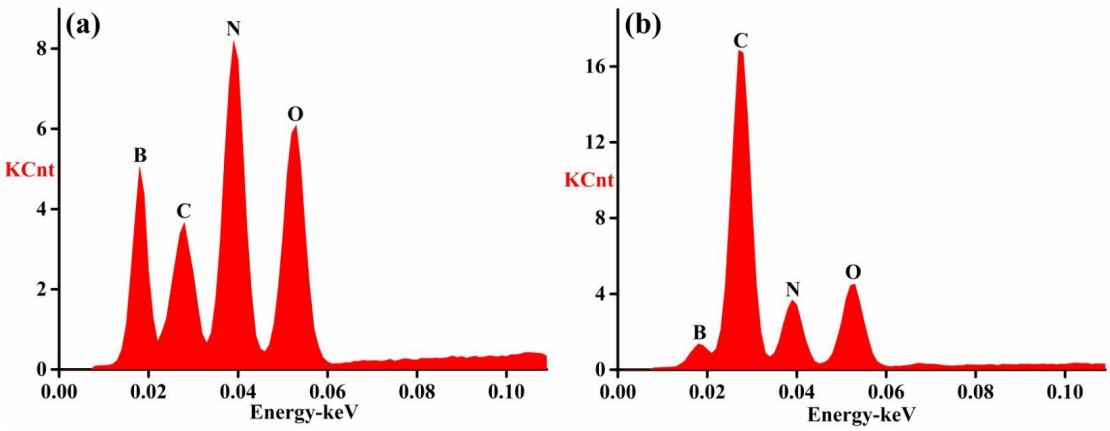

Fig. S2. EDAX spectra and analyses of (a) $BN(OH)_x$ and (b) $BN(OH)_x$-PrGO fillers.

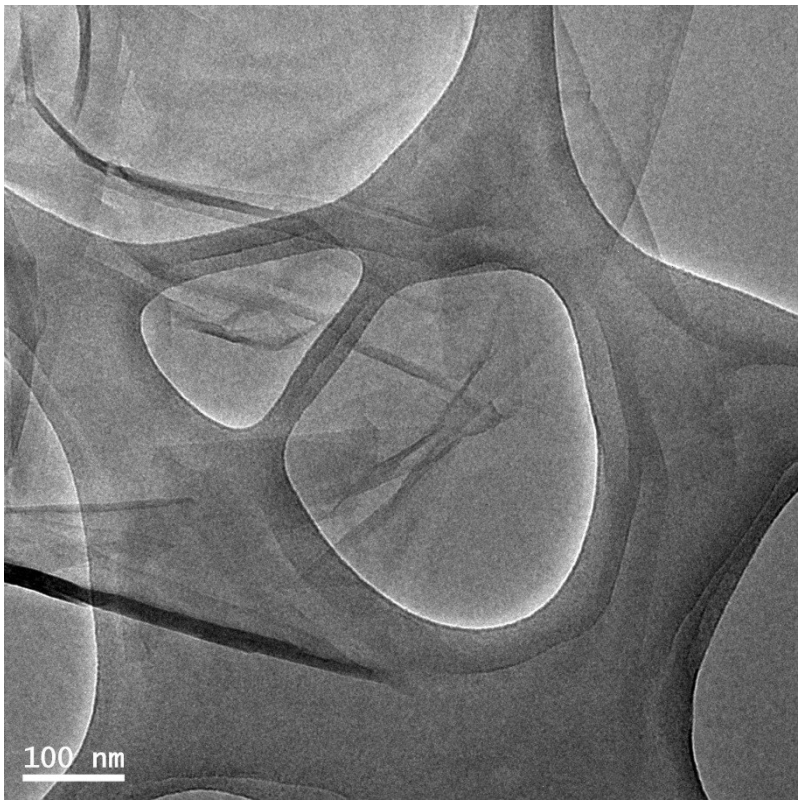

Fig. S3. TEM image of GO sheet.

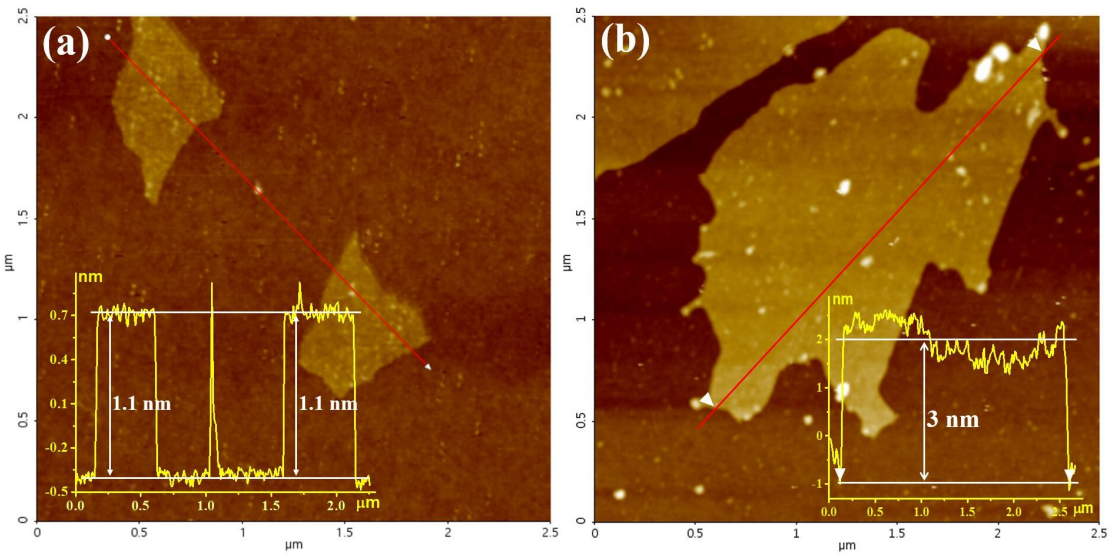

Fig. S4. AFM images of (a) GO, and (b) $BN(OH)_x$-PrGO fillers. The insets are the height profiles along the corresponding red lines that marked therein.

Table S1. Quantitative elemental compositions of the samples derived from XPS surveys.

Fillers	O (at %)	N (at %)	C (at %)	B (at %)	Chemical Formulas
$BN(OH)_x$	21.97	33.99	15.21	28.83	$BN_{1.2}O_{0.76}C_{0.53}$
$BN(OH)_x$-rGO	16.89	10.26	71.59	1.26	$BN_{8.1}O_{13.4}C_{56.8}$
$BN(OH)_x$-PrGO	15.44	20.83	55.01	8.72	$BN_{2.4}O_{1.8}C_{6.3}$

Characterization of PGO

The reduction and functionalization of GO by p-phenylenediamine (p-PD) is confirmed by Fourier transform infrared spectroscopy (FTIR) as shown in the Fig. S5. For GO, the bands at 3408, 1725, 1628, and 1055 cm^{-1} are due to the O−H bond of CO−H, C=O bond of a carboxyl group, the C=C bond of the aromatic ring, and C−O−C bond of epoxide group, respectively. After the modification with p-PD, the intensities of the peaks corresponding to the O−H, −COOH, and −C−O−C− bonds of pGO decrease in comparison to GO, suggesting the partial reduction of GO. Also, a new peak at 1176 cm^{-1} of C−N stretching vibration appears due to the formation of C−NH−C bond via nucleophilic substitution reaction between the epoxide groups of GO and the amine groups of p-PD [S4]. Besides, the peak (3219 cm^{-1}) of H-bonding interaction between oxygen-containing groups of GO and aminated groups of p-PD, as well as two new peaks (1554 and 727 cm^{-1}) of N−H stretching of $-C-NH_2$ groups support the functionalization of GO with p-PD.

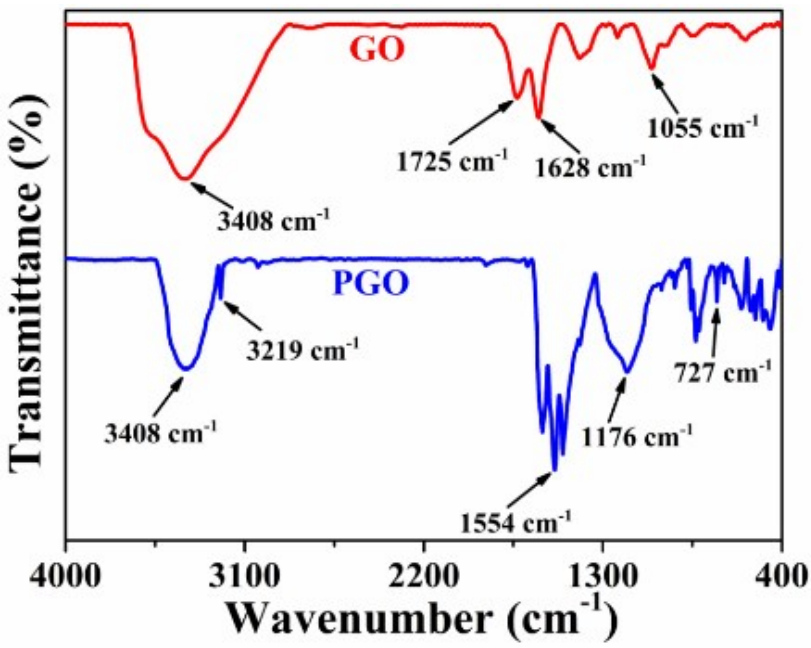

Fig. S5. FTIR spectra of GO and PGO.

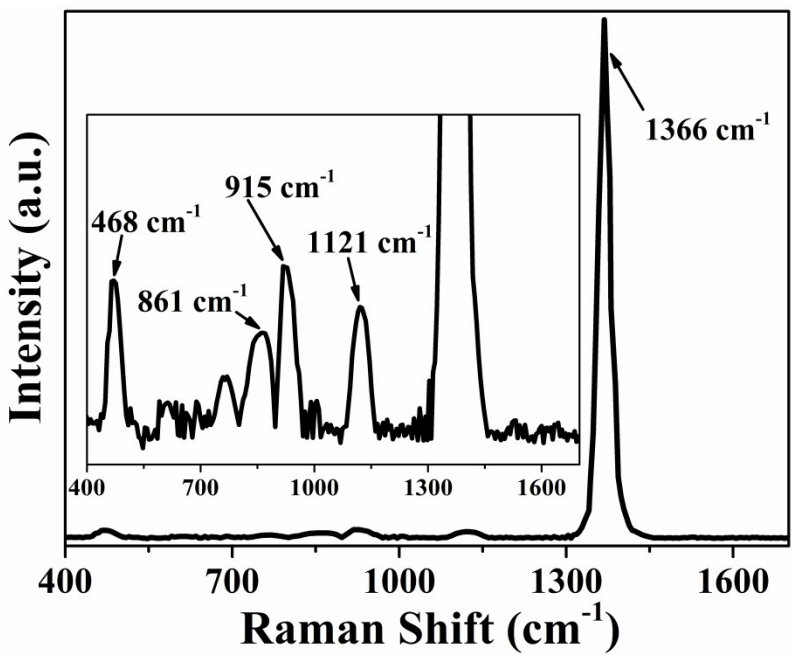

Fig. S6. Raman spectrum of $BN(OH)_x$ filler. The inset shows the full-scale expanded Raman spectrum of $BN(OH)_x$ filler.

Table S2. Mechanical and thermal properties of this work and their comparison with reported PU-based composite films.

Samples	Tensile strength (MPa)	Tensile modulus (MPa)	T_g (higher/lower) w.r.t present work based on DMA analysis	Storage modulus (higher/lower /comparable) w.r.t present work at -95 ^oC	Thermal stability (higher/lower/comparable) w.r.t present work based on initial degradation temp/char residue/maximum degradation temperature	Citation
APTMS-GO/WPU	27.79	-	-	-	lower	[S5]
APTES-GO/WPU	28.96	-	-	-	lower	
4 wt% GO/PU	<13	9.3	-	-	lower	[S6]
PU-4	36.3	-	-	lower	lower	[S7]
WPU-rGO 3 wt.%	23.9	615	-	-	-	[S8]
1 wt% HD-GNRs/PU	-	14.5	-	-	lower	[S9]
HPU/f-RGO2	37.6	128.5	-	-	comparable	[S10]
TPU/RGO-0.20	19.9	3.7	lower	higher	higher	[S11]
0.4 wt.% FGO/PU	19.6	~24.5	-	-	lower	[S12]
SHWPU/GO-4	27.1	-	lower	lower	lower	[S13]
PU-DA-GO3	28.55	38.76	-	-	-	[S14]
PU-DA-mGO3	35.60	40.6	-	-	-	
MWCNTs/PU	4	-	-	lower	-	[S15]
$GP_{0.1\%}$	-	-	-	-	comparable	[S16]
$GO_{0.1\%}$	-	-	-	-	lower	
TPU/PDA-GNP-1.0	34.1	27.8	lower	comparable	-	[S17]
TPU/GNP-1.0	8.8	36.7	lower	comparable	-	
$^3BN(OH)_x$-PrGO/PU	87.9	91.3	3 ºC	2663 MPa	-	This work

Calculation of permeability (*P*), diffusivity (*D*), and solubility (*S*) Coefficients

P was calculated according to equation S1:

$$P = \frac{O_2GTR \cdot l}{cmHg} \tag{S1}$$

Where, *l* is the thickness of the film, and cmHg is the unit for the pressure gradient pass through the prepared film.

D was calculated according to equation S2 [S18,S19]:

$$D = \frac{l^2}{7.199 \cdot t_{1/2}} \tag{S2}$$

Where $t_{1/2}$ (in seconds) is half of the time to reach steadiness O_2GTR value.

S was calculated according to equation S3:

$$S = \frac{P}{D} \tag{S3}$$

Table S3. O_2GTR and O_2 transmission coefficient values of all the films.

Samples	O_2GTR (cc/m^2·d·atm)	Thickness of Films (cm)	Permeability Coefficient (cc·cm/m^2·d·atm)	Diffusion Coefficient (cm^2/s) (10^{-8})	Solubility Coefficient (cc/cm^3·atm) (10^{-1})
PU	2120	0.0092	19.50	9.11	2.48
[1]BN(OH)$_x$/PU	808	0.0099	8.00	6.84	1.35
[1]BN(OH)$_x$-rGO/PU	723	0.0101	7.30	6.33	1.34
[2]BN(OH)$_x$-rGO/PU	750	0.0104	7.80	6.62	1.36
[1]BN(OH)$_x$-PrGO/PU	397	0.0094	3.73	6.23	0.69
[2]BN(OH)$_x$-PrGO/PU	289	0.0094	2.72	5.56	0.57
[3]BN(OH)$_x$-PrGO/PU	201	0.0096	1.93	4.61	0.48
[4]BN(OH)$_x$-PrGO/PU	280	0.0095	2.66	5.51	0.56

Table S4. O_2GTR and *P* values of this work and their comparison with reported filler based polymer films.

Samples	Polymer matrix	Filler name (loading)	*P* or OTR	% of decrease of *P* compared to polymer matrix	Citation
DDA-rGO1-4/PU	PU	DDA-rGO1 (4 wt%)	37 cc mm m^{-2} d^{-1} atm^{-1}	84	[S19]
DDA-rGO2-4/PU		DDA-rGO2 (4 wt%)	46 cc m m^{-2} d^{-1} atm^{-1}	80	
GONS/PLA	PLA	GONS (1.37 vol%)	1.145×10^{-14} cm^3 cm cm^{-2} s^{-1} Pa^{-1}	45	[S20]
RC/5 wt% GNP	RC	GNP (5 wt%)	~0.8×10^{-18} m^3 m m^{-2} s^{-1} Pa^{-1}	27	[S21]
PGN	PS	Phenyl isocyanate-treated graphite oxide (2.27 vol%)	1.84 barrer	61	[S22]
PMMA/GO	PMMA	GO (5 wt%)	~ .24 ml/[m^2.day.atm]	90.4	[S23]
LDG-5	LLDPE	DA-G (5 wt%)	19.5 fm/Pa.S	47	[S24]
PLA+GNP	PLA	GNP (0.4 wt%)	1.20×10^{-18} m^2 s^{-1} Pa^{-1}	68	[S25]
PAGCs05	PANI	ABF-G (0.5 wt%)	0.1056 barrer	86	[S26]
PND/AFG	PND	AFG (5 wt%)	~25 cc/m^3 day	79.3	[S27]
Nylon11/FG	Nylon11	FG (0.3 wt%)	10.1 cc/(m^2 day)	47	[S28]
Nylon12/FG	Nylon12		10.2 cc/(m^2 day)	30.4	
PS/pv-GO2	PS	Pv-GO (2 wt%)	2.24 Barrier	25	[S29]
HPGN	PMMA	PGN (0.5 wt%)	0.81 Barrier	70	[S30]
GO/XNBR	XNBR	GO (1.9 vol%)	~1.5×10^{-17} m^2 Pa^{-1} s^{-1}	55	[S31]

GE/SBR	SBR	GE (7 phr)	N/A	87.8	[S32]
CS/B/1GO-T	CS	GO (1 wt%)	0.34×10^{-15} cm^3 cm cm^{-2} s^{-1} Pa^{-1}	~86.1	[S33]
PVA/GO	PVA	GO (0.07 vol%)	~ 0.0035 cc m^{-2} day^{-1}	~82	[S34]
NFrGO-CANC	CANC	NFrGO (0.5 wt%)	22.75 cc mm m^{-2} d^{-1} atm^{-1}	66	[S35]
$^3BN(OH)_x$-PrGO/PU	PU	$BN(OH)_x$-PrGO (3 wt%)	1.93 cc·cm/m^2·d·atm	90.1	This work

Calculation of dielectric constant (ε')

Measurements of the samples were done as a function of frequency (1000 Hz to 1 MHz) at 30 ^oC. To measure the dielectric constant (ε'), a capacitor is fabricated using PU film or $BN(OH)_x$-PrGO/PU composite films as ε'. A layer of silver was coated on both sides of the film to serve as electrodes. The ε' can be evaluated using the equation S4 [S36]:

$$\varepsilon' = \frac{C_p \times d}{\varepsilon_o \times A} \tag{S4}$$

Where, C_p, d, and A are the capacitance, thickness, and area of cross-section, respectively and ε_o (= 8.854 x 10^{-12} F/m) is the permittivity of the free space.

Calculation of corrosion rate (*CR*) and corrosion protection efficiency (*IE*)

CR is calculated using the following equation S5 [S37,S38]:

$$CR = \frac{I_c(A/cm^2) \cdot M(g)}{D(g/cm^3) \cdot V} \tag{S5}$$

where *V* is the valence, *M* is the molecular weight, 3270 is a constant, and *D* is the density.

IE is calculated from the following equation S6:

$$IE\% = \frac{I_{c,s} - I_{c,c}}{I_{c,s}} \tag{S6}$$

where, $I_{c,s}$ and $I_{c,c}$ are the corrosion current of bare steel, and the coated specimen, respectively.

Table S5. Potentiodynamic polarization parameter values for bare steel and nanocomposite-coated steel.

Samples	E_P[a] (mV)	I_c[b] (μA/cm^2)	*CR*[c] (mm/year)	*IE*[d] (%)
Steel	-948	13.02	0.152	-
PU	-352	0.23	2.71×10^{-3}	98.21
[1]BN(OH)$_x$-PrGO/PU	-111	4.14×10^{-2}	4.83×10^{-4}	99.68
[2]BN(OH)$_x$-PrGO/PU	18	8.61×10^{-3}	1.00×10^{-4}	99.93
[3]BN(OH)$_x$-PrGO/PU	92	5.26×10^{-3}	6.14×10^{-5}	99.96

[a] corrosion potential, [b] corrosion current, [c] corrosion rate, [d] corrosion protection efficiency.

Table S6. Summary of anti-corrosion properties of various polymer composites obtained from the literature.

Anti-corrosion Samples	*CR* (mm/year)	*IE* (%)	Citation
EVOH/15BA/5GO	3.43×10^{-3}	98.46	[S38]
PAGCs05	4.4×10^{-3}	53.49	[S26]
60% mGO-ODA/MAPP	2.26×10^{-3}	99.15	[S39]
h-BN/PVA	1.19×10^{-3}	-	[S40]
PPCc10	1.16×10^{-4}	99.98	[S41]
HPGN	8.64×10^{-3} [a]	99.68	[S30]
PS/pv-GO_2	4.29×10^{-3} [a]	99.53	[S29]
steel−PANI@BN/PVA	0.007	99.30	[S42]
GPCc	6.99×10^{-7}	97.3	[S43]
DE/TiO_2/rGO	-	96.78	[S44]
$^{3}BN(OH)_x$-PrGO/PU	6.14×10^{-5}	99.96	This work

[a] Already unit conversion.

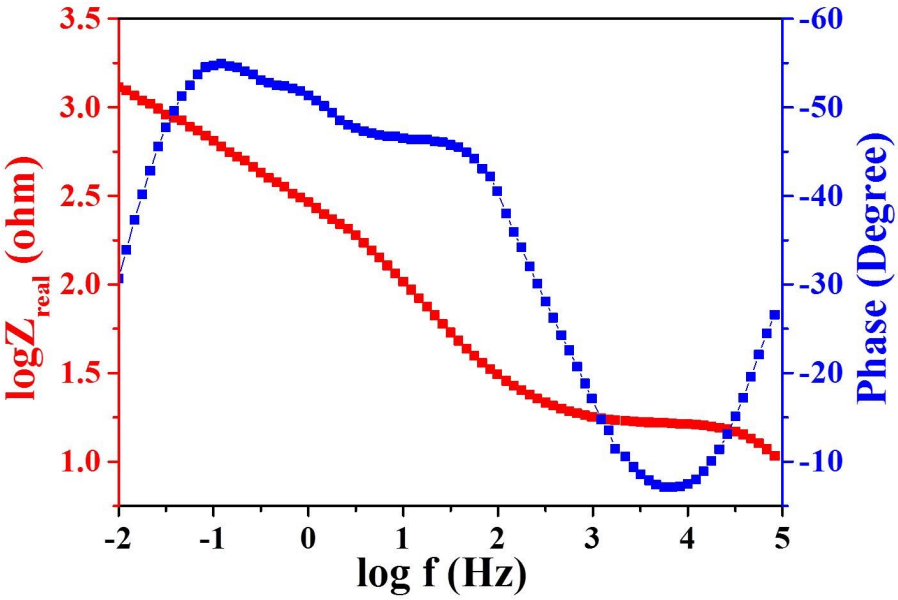

Fig. S7. Bode and Phase plots of bare steel substrate after 0.5 h immersion in 3.5 wt% NaCl solution.

References:

S1 P. Bandyopadhyay, W. B. Park, R. K. Layek, M. E. Uddin, N. H. Kim, H. G. Kim and J. H. Lee, *J. Memb. Sci.*, 2016, **500**, 106–114.

S2 P. Bandyopadhyay, T. T. Nguyen, N. H. Kim and J. H. Lee, *Chem. Eng. J.*, 2018, **333**, 170–184.

S3 W. S. Hummers and R. E. Offeman, *J. Am. Chem. Soc.*, 1958, **80**, 1339–1339.

S4 H. L. Ma, H. B. Zhang, Q. H. Hu, W. J. Li, Z. G. Jiang, Z. Z. Yu and A. Dasari, *ACS Appl. Mater. Interfaces*, 2012, **4**, 1948−1953.

S5 L. Hu, P. Jiang, P. Zhang, G. Bian, S. Sheng, M. Huang, Y. Bao and J. Xia, *J. Mater. Sci.*, 2016, **51**, 8296–8309.

S6 D. Cai, J. Jin, K. Yusoh, R. Rafiq and M. Song, *Compos. Sci. Technol.*, 2012, **72**, 702–707.

S7 X. Wang, Y. Hu, L. Song, H. Yang, W. Xing and H. Lu, *J. Mater. Chem.*, 2011, **21**, 4222–4227.

S8 N. Yousefi, M. M. Gudarzi, Q. Zheng, X. Lin, X. Shen, J. Jia, F. Sharif and J. K. Kim, *Compos. Part A*, 2013, **49**, 42–50.

S9 C. Xiang, P. J. Cox, A. Kukovecz, B. Genorio, D. P. Hashim, Z. Yan, Z. Peng, C. C. Hwang, G. Ruan, E. L. G. Samuel, P. M. Sudeep, Z. Konya, R. Vajtai, P. M. Ajayan and J. M. Tour, *ACS Nano*, 2013, **7**, 10380–10386.

S10 S. Thakur and N. Karak, *ACS Sustain. Chem. Eng.*, 2014, **2**, 1195−1202.

S11 M. Bera and P. K. Maji, *Polymer*, 2017, **119**, 118−133.

S12 Q. Jing, W. Liu, Y. Pan, V. V. Siberschmidt, L. Li and Z. Dong, *Materials Design*,

2015, **85**, 808–814.

S13 T. Wan and D. Chen, *Prog. Org. Coat.*, 2018, **121**, 73–79.

S14 C. Lin, D. Sheng, X. Liu, S. Xu, F. Ji, L. Dong, Y. Zhou and Y. Yang, *Polymer*, 2017, **127**, 241–250.

S15 S. Li, X. Du, C. Hou, X. Hao, J. Jia, T. Guan, T. Yi and G. Ma, *Compos. Sci. Technol.*, 2017, **143**, 46–55.

S16 L. Cristofolini, G. Guidetti, K. Morellato, M. Gibertini, M. Calvaresi, F. Zerbetto, M. Montalti and G. Falini, *ACS Omega*, 2018, **3**, 8829−8835.

S17 K. Chen, Q. Tian, C. Tian, G. Yan, F. Cao, S. Liang and X. Wang, *Ind. Eng. Chem. Res.*, 2017, **56**, 11827−11838.

S18 K. D. Ziegel, H. K. Frensdorft and D. E. Blair, *J. Polym. Sci., Part A-2: Polym. Phys.*, 1969, **7**, 809−819.

S19 T. T. Nguyen, P. Bandyopadhyay, X. Li, N. H. Kim and J. H. Lee, *J. Membr. Sci.*, 2017, **540**, 108–119.

S20 H. D. Huang, P. G. Ren, J. Z. Xu, L. Xu, G. J. Zhong, B. S. Hsiao and Z. M. Li, *J. Membr. Sci.*, 2014, **464**, 110–118.

S21 S. Mahmoudian, M.U. Wahit, M. Imran, A. Ismail, H. Balakrishnan, *J. Nanosci. Nanotechnol.*, 2012, **12**, 5233–5239.

S22 O.C. Compton, S. Kim, C. Pierre, J.M. Torkelson, S.T. Nguyen, *Adv. Mater.*, 2010, **22**, 4759–4763.

S23 S. Morimune, T. Nishino, T. Goto, *ACS Appl. Mater. Interfaces,* 2012, **4**, 3596–3601.

S24 T. Kuila, S. Bose, A.K. Mishra, P. Khanra, N.H. Kim, J.H. Lee, *Polym. Test*., 2012, **31**, 31–38.

S25 A.M. Pinto, J. Cabral, D.A.P. Tanaka, A.M. Mendes, *Polym. Int*., 2013, **62**, 33–40.

S26 C. H. Chang, T. C. Huang, C.-W. Peng, T. C. Yeh, H. I. Lu, W. I. Hung, C. J. Weng, T. I. Yang, J. M. Yeh, *Carbon,* 2012, **50**, 5044–5051.

S27 D. Lee, M. C. Choi and C. S. Ha, *J. Polym. Sci., Part A: Polym. Chem.*, 2012, **50**, 1611–1621.

S28 J. Jin, R. Rafiq, Y.Q. Gill, M. Song, *Eur. Polym. J*., 2013, **49**, 2617–2626.

S29 Y. H. Yu, Y. Y. Lin, C. H. Lin, C. C. Chan, Y. C. Huang, *Polym. Chem*., 2014, **5**, 535–550.

S30 K. C. Chang, W. F. Ji, M. C. Lai, Y. R. Hsiao, C. H. Hsu, T. L. Chuang, Y. Wei, J. M. Yeh, W. R. Liu, *Polym. Chem*., 2014, **5**, 1049–1056.

S31 H. Kang, K. Zuo, Z. Wang, L. Zhang, L. Liu, B. Guo, *Compos. Sci. Technol*., 2014, **92**, 1–8.

S32 W. Xing, M. Tang, J. Wu, G. Huang, H. Li, Z. Lei, X. Fu, H. Li, *Compos. Sci. Technol*., 2014, **99**, 67–74.

S33 N. Yan, F. Capezzuto, M. Lavorgna, G. G. Buonocore, F. Tescione, H. Xia and L. Ambrosio, *Nanoscale*, 2016, **8**, 10783–10791.

S34 J.T. Chen, Y. J. Fu, Q.F. An, S. C. Lo, Y. Z. Zhong, C. C. Hu, K. R. Lee, J. Y. Lai, *Carbon,* 2014, 75, 443–451.

S35 M. E. Uddin, R. K. Layek, H. Y. Kim, N. H. Kim, D. Hui, J. H. Lee, Compos.

Part B-Eng., 2016, **90**, 223–231.

S36 S. Thakur, P. Bandyopadhyay, S. H. Kim, N. H. Kim and J. H. Lee, *Compos. Part A*, 2018, **110**, 284−293.

S37 R. X. Yuan, S. Q. Wu, P. Yu, B. H. Wang, L. W. Mu, X. G. Zhang, Y. X. Zhu, B. Wang, H. Y. Wang and J. H. Zhu, *ACS Appl. Mater. Interfaces*, 2016, **8**, 12481–12493.

S38 X. Li, P. Bandyopadhyay, M. Guo, N. H. Kim and J. H. Lee, *Carbon*, 2018, **133**, 150–161.

S39 X. Li, P. Bandyopadhyay, T. T. Nguyen, O. Park and J. H. Lee, *J. Membr. Sci.*, 2018, **547**, 80–92.

S40 E. Husain, T. N. Narayanan, J. J. T. Tijerina, S. Vinod, R. Vajtai and P. M. Ajayan, *ACS Appl. Mater. Interfaces*, 2013, **5**, 4129−4135.

S41 X. Sheng, W. Cai, L. Zhong, D. Xie and X. Zhang, *Ind. Eng. Chem. Res.*, 2016, **55**, 8576−8585.

S42 N. Sarkar, G. Sahoo, R. Das, G. Prusty, D. Sahu and S. K. Swain, *Ind. Eng. Chem. Res.*, 2016, **55**, 2921−2931.

S43 W. Sun, L. Wang, T. Wu, Y. Pan and G. Liu, *Carbon*, 2014, **79**, 605–614.

S44 M. J. Nine, M. A. Cole, L. Johnson, D. N. H. Tran and D. Losic, *ACS Appl. Mater. Interfaces*, 2015, **7**, 28482−28493.